FVCOM model estimate of the location of Air France 447

Changsheng Chen, Richard Limeburner, Guoping Gao, Qichun Xu, Jianhua Qi, Pengfei Xue, Zhigang Lai, Huichan Lin, Robert Beardsley, Breck Owens, et al.

Ocean Dynamics
Theoretical, Computational and Observational Oceanography

ISSN 1616-7341

Ocean Dynamics
DOI 10.1007/s10236-012-0537-5

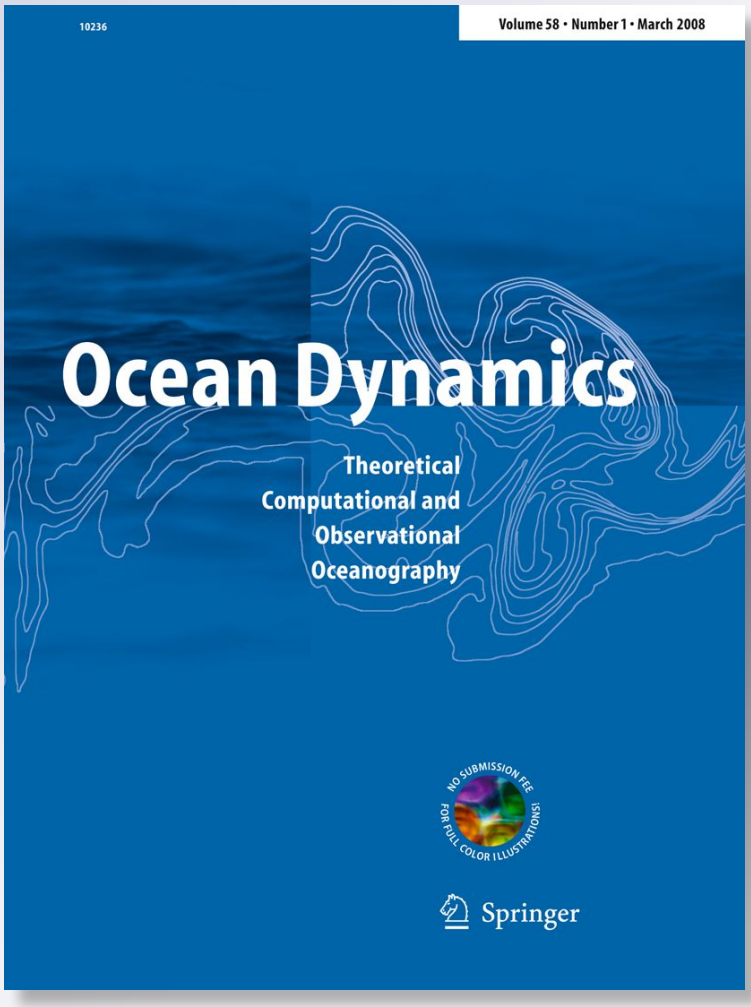

Springer

Ocean Dynamics
DOI 10.1007/s10236-012-0537-5

FVCOM model estimate of the location of Air France 447

Changsheng Chen · Richard Limeburner · and members of the UMASS-D FVCOM Group · Guoping Gao · Qichun Xu · Jianhua Qi · Pengfei Xue · Zhigang Lai · Huichan Lin · and members of the WHOI Field Measurement Group · Robert Beardsley · Breck Owens · Barry Carlson

Received: 10 June 2011 / Accepted: 6 March 2012

Abstract On June 1, 2009, Air France AF447 disappeared in the Equatorial Atlantic Ocean en route from Rio de Janeiro, Brazil, to Paris, France. On June 6–19, 2009, bodies and debris from the aircraft were recovered floating in the equatorial ocean. This paper describes efforts on using the global–local nested finite volume community ocean model (FVCOM) to model reversely the tracks of bodies and debris back to the time of the crash and to help searchers locate the cockpit voice and flight data recorders and learn why this tragic accident occurred. To validate the reliability and reality of FVCOM, eight surface drifters were deployed by the French Bureau d'Enquêtes et d'Analyses pour la sécurité de l'aviation civile (BEA) near the last known position in early June 2010 for a period of 3 weeks. These drifter data were used to optimize the spatial and temporal correlation scales of the adaptive sampling data assimilation method of FVCOM. Applying an optimized FVCOM system to assimilate all available drifter- and float-tracking-derived currents in May–June 2009 under three different wind conditions, we reproduced the June 2009 current fields in the area near the LKP and used these fields to reversely track bodies and debris from locations where they were found to the time when the crash occurred. Possible locations for the crashed plane were suggested based on our model results and were made available to the French investigators and the Woods Hole Oceanographic Institution REMUS autonomous underwater vehicle Operations Group who successfully located the aircraft debris field in April 2011 on the seafloor at a depth of 3,900 m.

Keywords Air France 447 · AF447 · FVCOM · Global–regional nested FVCOM system · FVCOM unstructured grid finite volume coastal ocean model · UMASS-D · SMAST · WHOI · BEA · Airbus 330

Responsible Editor: Oyvind Breivik

This article is part of the Topical Collection on *Advances in Search and Rescue at Sea*

C. Chen · G. Gao · Q. Xu · J. Qi · P. Xue · Z. Lai · H. Lin
School for Marine Science and Technology,
University of Massachusetts-Dartmouth (UMASS-D),
New Bedford, MA 02744, USA

C. Chen · R. Limeburner (✉) · R. Beardsley · B. Owens
Department of Physical Oceanography,
Woods Hole Oceanographic Institution (WHOI),
Woods Hole, MA 02543, USA
e-mail: rlimeburner@whoi.edu

B. Carlson
New Plymouth, New Zealand

1 Introduction

On June 1, 2009, Air France AF447 disappeared in the Equatorial Atlantic Ocean en route from Rio de Janeiro, Brazil, to Paris, France. On June 6–19, 2009, bodies and debris from the aircraft were recovered floating in the equatorial ocean. A total of four searches, coordinated by the French Bureau d'Enquêtes et d'Analyses pour la sécurité de l'aviation civile (BEA), were carried out to locate the crashed plane. Ocean models were used in third and fourth searches to assist the search by predicting the paths of floating bodies and debris recovered many days after the accident backwards in time to the time and location of the accident. We applied the global–local nested finite volume community ocean model (FVCOM) to predict possible locations for the crashed plan for the third and fourth searches; the results were made available to the Woods Hole

Published online: 21 March 2012

Oceanographic Institution (WHOI) REMUS autonomous underwater vehicle (AUV) Operations Group who successfully located the aircraft debris field in April 2011.

Tracking bodies and debris backwards in time requires the three-dimensional flow and surface wind fields in the accident region. The last known position (LKP) of AF447 was at −30.59° W and 2.98° N. This location is in the Atlantic equatorial region (Fig. 1). On June 1, 2009, the only available ocean data were 6 Atlantic Oceanographic and Meteorological Laboratory (AOML) 15-m drifter buoys, 9 ARGO free-drifting profile floats, and 12 fishermen (BF or SF) drifter buoys covering the region between 21° W to 35° W and 0° to 7° N. Note that the ARGO floats rose to the surface every 10 days and transmitted data and position approximately hourly over about 12 h. In particular, a fisherman drifter named SF246 moved near (<7 km) the LKP of the plane on June 5, 2009. According to drifter trajectories, the Northern Equatorial Current appeared around 4° N or higher, and the currents in the surrounding area of LKP varied significantly with time and space.

To reproduce the surface currents in that area and thus determine a possible location of AF447, one requires to (1) have accurate meteorological forcing (winds, air pressure, and heat flux, etc.), (2) resolve mesoscale variability of the sea surface elevation (or sea surface height, SSH), and (3) capture the spatial and temporal structures of the surface mixed layers. The difficulties, however, are that the area are located in the variation range of the Intertropical Convergence Zone (ITCZ) in which no well-validated meteorological forcing conditions were available. The winds from three sources (the satellite-derived blended winds, http://www.ncdc.noaa.gov/oa/rsad/air-sea.html/; NCEP reanalysis global winds, https://dss.ucar.edu/datazone/dsszone/ds083.2/index.html; and ECMWF global winds) significantly differed in direction (Fig. 2). The satellite-derived sea surface temperature (SST) and SSH were available daily over the global scale, with space resolutions of ~8 and ~30 km, respectively. The 30-km resolution in SSH would not be able to resolve the short-term mesoscale variation of currents in that area.

Due to so many uncertainties and the lack of sufficient data, we have used an ensemble approach shown in Fig. 3 for the modeling exercise. The ensemble approach allows us to estimate the influences of various winds on currents and thus on the final determination of the possible location of AF447. To resolve the wind-driven mesoscale variability of the surface current around the LKP, we used wind data from the European Center for Medium Range Forecasting (ECMWF), satellite blended wind fields, and, in addition, set up a mesoscale weather research and forecast (WRF) model to reproduce the high-resolution wind field in the study region. The model experiments were made using the following procedure: first, we spun up a global-FVCOM from January 1 to June 30, 2009, and then started running the local-domain high-resolution FVCOM driven by three types of wind forcing with a nested boundary condition specified by the global-FVCOM model output from May 1 to June 30, 2009. The flow field predicted by the high-resolution FVCOM was used to track bodies and debris reversely to the time of plane crash.

This paper describes methodologies used in our ensemble approach and summarizes our major finding. The remaining sections are organized as follows. In Section 2, the structures of the global–local nested FVCOM system and the designs of numerical experiments are described. In Section 3, the results of the model validation are presented and discussed. In Section 4, the model-predicted location of AF447 is presented. In Section 5, conclusions are summarized. Note that the BEA has never released the actual location of AF447 on the seafloor, but they did release a

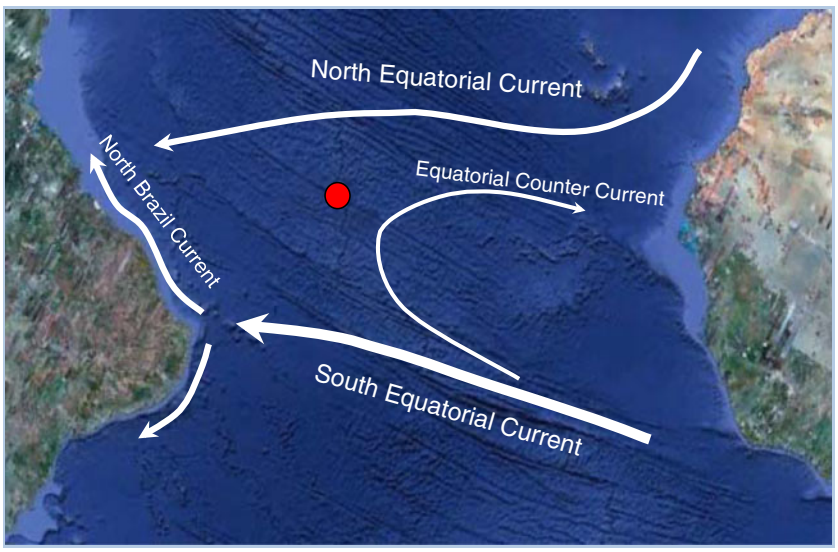

Fig. 1 Schematic of the regional circulation and the last known position (*red dot*) of AF447 at 30.59° W and 2.98° N

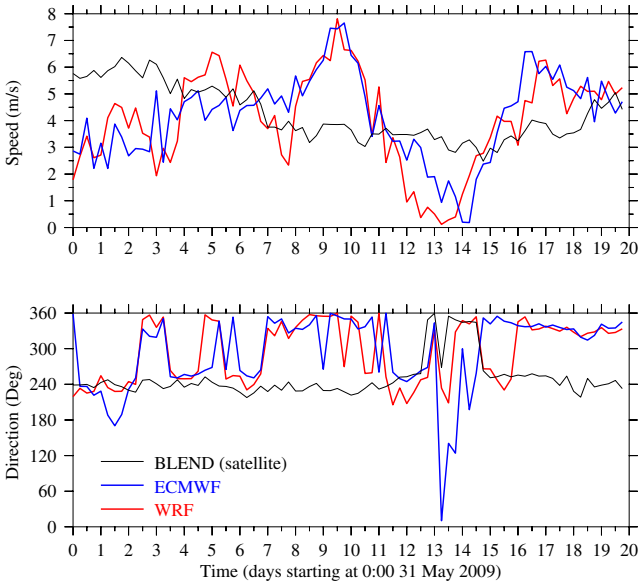

Fig. 2 Comparison of the BLEND, ECMWF, and WRF wind speeds and directions at a location of 30.53° W and 2.6° N over the period May 31–June 20, 2009

graphical location to the press. We present the distance between the model-predicted and the BEA graphical locations of AF447 in Section 4.

2 The model and designs of numerical experiments

2.1 The global/local-domain FVCOM system

The model used for the AF447 search is FVCOM, an unstructured grid, three-dimensional primitive equations fully current–wave–ice coupled finite volume community ocean model. This model was developed originally by Chen et al. (2003) and modified and upgraded by a joint effort of the University of Massachusetts-Dartmouth (UMASS-D) and WHOI (Chen et al. 2006a, b). FVCOM is governed by seven primitive equations of momentums, continuity, temperature, salinity, and density in the spherical coordinate, with turbulent mixing parameterized by the general ocean turbulence model (Burchard 2002) in the vertical and Smagorinsky turbulent closure scheme in the horizontal (Smagorinsky 1963). The flux forms of the governing equations are discretized in the unstructured triangular mesh in the horizontal (Chen et al. 2003) and in the generalized terrain-following coordinate in the vertical (Pietrzak et al. 2002). FVCOM is integrated with options of various mode split and semi-implicit schemes in time and the second-order accurate advection schemes in space. The unstructured grid finite volume methods combine the best attributes of the finite difference method for simple discrete computational efficiency and the finite element methods for geometric flexibility. The flux computational approach provides an accurate representation of mass, heat, and salt conservation.

A global/local-domain nested FVCOM system was developed for this purpose. This system consists of two FVCOMs: the global-FVCOM and the local-domain FVCOM. Global-FVCOM is a coupled hydrodynamics and ice model covering the entire global oceans with the inclusion of all major rivers. The computational domain is configured with the non-overlapped triangular grid with the horizontal resolution from 5 to 50 km (Fig. 4). The total numbers of triangular cells and nodes are 425,146 and 217,436, respectively. The hybrid coordinate (Pietrzak et al. 2002) is used in the vertical, with a total of 45 layers, 10 and 5 uniform layers near the surface and bottom in the region deeper than 225 m, respectively, and then transfers to the sigma coordinate in the shallow continental and coastal regions. The thickness of the uniform layer is 5 m, so the hybrid coordinate is transited at the location where all layers have a uniform thickness of 5 m. This hybrid coordinate approach allows us to avoid the numerical error in the simulation of surface mixed layer and bottom boundary

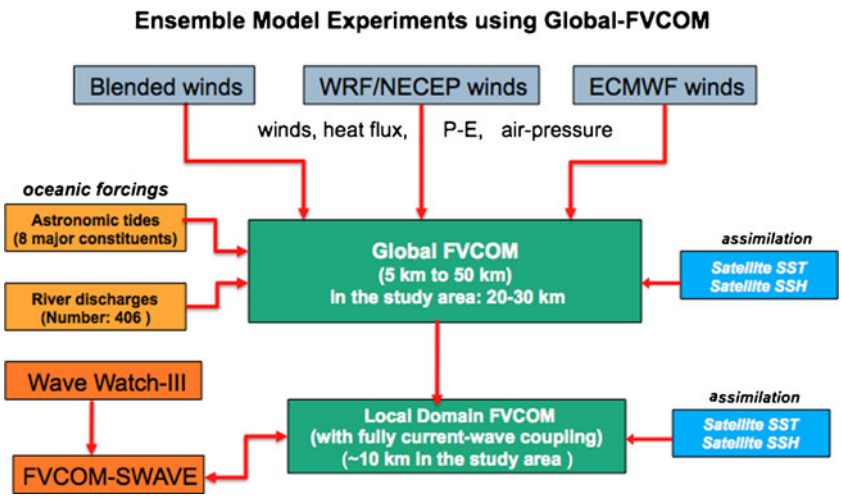

Fig. 3 Flowchart of the ensemble model approach used for the AF447 modeling experiments. *FVCOM*—unstructured grid, finite-volume community ocean model. *FVCOM-SWAVE*—unstructured version of the surface wave model (*SWAN*) developed by the FVCOM team

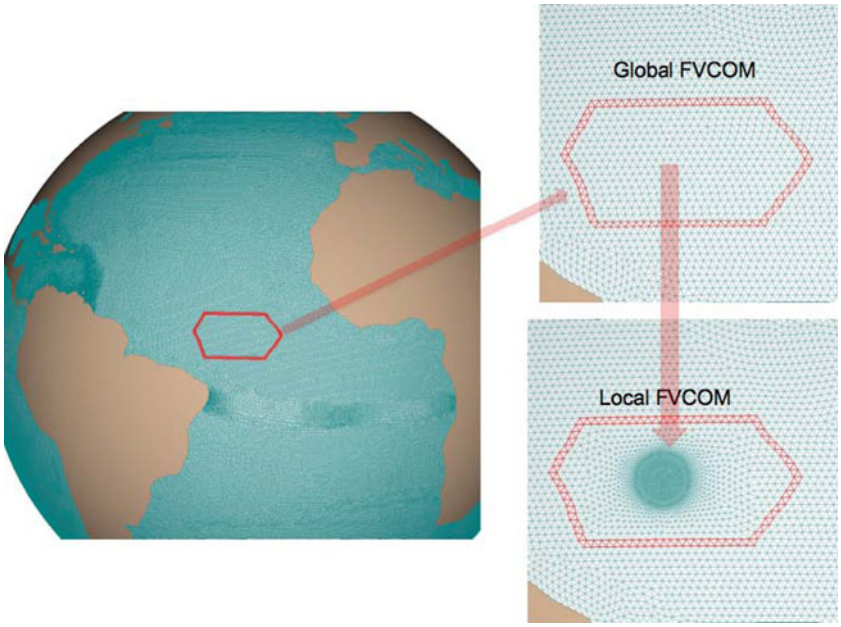

Fig. 4 Schematic of the grid and nested boundary of global- and local-domain FVCOMs. *Triangles* marked by the *red color* are the nested boundaries. Horizontal resolution in the global domain was 20–30 km and in the local domain is 7–10 km

layer in the interior at no sacrifice or loss of the vertical resolution in the shallower coastal region. Global-FVCOM is solved numerically using the semi-implicit scheme with a time step of 600 s.

The local-domain FVCOM is a high-resolution grid model nested with global-FVCOM (Fig. 4). The grid configuration is the same as global-FVCOM in the vertical and refined up to 7–10 km in the horizontal near the LKP. It is coupled with global-FVCOM through the nesting boundary where both global and local domains share the common grids. This nesting approach does not require the interpolation of physical variables from one to another like a structured grid model does.

The bathymetric data used for both global- and local-domain FVCOMs were taken from two sources: the sub-Arctic region (up to 72° N) is represented by depths from the 2-min Naval Oceanographic Office Digital Bathymetric Data Base–variable resolution, version 4.3, and the central Arctic bathymetry is obtained from the International Bathymetric Chart of the Arctic Ocean, a digital database that contains all available bathymetric data north of 64° N. These two data sets match very well in the overlapping region between 64° N and 72° N. The vertical maximum depth is 5,500 m and the minimum depth at the coast is 5 m.

Global-FVCOM is driven by (1) astronomic tidal forcing, (2) surface wind stress, (3) net heat flux at the surface plus shortwave irradiance in the water column, (4) the sea level pressure gradient, (5) precipitation minus evaporation, and 6) river discharges. Eight tidal constituents are included to build the tidal potential with the inclusion of various corrections due to the Earth tide and ocean loading: M_2, S_2, N_2, K_2, K_1, P_1, O_1, and Q_1. The local-domain FVCOM was driven by the same forcings as global-FVCOM with the boundary conditions specified using the simultaneously output of global-FVCOM. Both global- and local-domain FVCOM experiments include the optimal interpolation data assimilation for SST, SSH, and current derived from drifters. Data assimilations were run with a 3-h window and with the predefined correlation scale of 50 km. These two scales were determined based on the spatial scales determined from drifters for local currents and the North Equatorial Current. With calibrated mixed layer depths from ARGO floats, we combined all drifter-derived currents as the surface current since they were all in the surface mixed layer.

To resolve the wind-induced mesoscale variability of currents, we applied a mesoscale WRF model to reproduce the high-resolution wind field for the local-domain FVCOM. The WRF was configured through two-way nested approaches from domain I (27 km) to domain II (9 km). The 9-km model output was used to drive a local FVCOM domain. The heat flux calculation in WRF used the modified algorithm proposed and implemented by Chen et al. (2005). This algorithm provides a more accurate estimation of sensible and latent heat fluxes at the sea surface.

2.2 Designs of numerical experiments

The model was initialized using the global-FVCOM 50-year spin-up model output field on January 1, 2009, and run until June 30, 2009, under three different wind fields (Blended, NECEP/WRF, and ECMWF), respectively. The surface heat flux, shortwave irradiance, precipitation minus evaporation, and sea surface pressure used in the model were from NCEP reanalysis fields. Experiments were focused on the local high-resolution domain: (a) hydrodynamic model runs under three types of wind forcing and (b) the current–wave interaction model run under three types of wind forcing.

Blended winds were downloaded from the web site http://www.ncdc.noaa/gov/oa/rsad/air-sea.html, the ECMWF winds were provided by the ECMWF team for the AF447 search, and the WRF winds were from the high-resolution WRF model run.

The reverse body and debris tracking was approached using a three-dimensional Lagrangian tracking program as

$$P_n\left(\vec{x}_{t-\Delta t}, t-\Delta t\right) = -\int_{t}^{t-\Delta t} \left(\vec{v} + \alpha \vec{w}\right) \mathrm{d}t + P_n\left(\vec{x}_t, t\right) \quad (1)$$

where $P_n\left(\vec{x}_{t-\Delta t}, t-\Delta t\right)$ and $P_n\left(\vec{x}_t, t\right)$ are the locations of the nth individual body or debris at the time of $t-\Delta t$ and t, $\vec{v}$ is the three-dimensional velocity vector, $\vec{w}$ is the wind velocity vector, and α is the wind drag factor considered in the tracking. The reverse distance was calculated by a modified fourth-order Runge–Kutta time-stepping scheme with second-order accuracy (Chen et al. 2003). Experiments were made for the cases with the wind drag factors of 0, 1, 2, and 3 %. Different wind drags were used since the submergence of the individual floating debris was unknown. The effect of the warm seawater temperatures on the submergence of the bodies was also an unknown factor affecting the submergence.

The model-predicted flow field was validated by comparisons with drifter trajectories available around the LKP in June 2009. Since all drifter and float data were assimilated into the model, the data assimilation results were sensitive to the spatial correlation scale used in the optimal interpolation assimilation method. To help a model determine the reasonable spatial correlation scale that is capable of resolving the mesoscale variation of currents, in June 2010, the BEA deployed nine Iridium/GPS surface drifters with Davis drogues in a regular grid pattern within 40 nautical miles of the LKP of AF447. Eight of these drifters showed that the surface circulation patterns in June, even though for a different year, varied significantly in space and time (Fig. 5). This suggests that it was not possible to use either climatologic flow field or fields in different years to determine the possible location of the airplane on the seafloor.

Assimilating the comprehensive drifter data collected in 2010 into the model, we reran the global/local-domain FVCOM for the year 2010 to determine under what correlation scale the high-resolution local-domain FVCOM could reproduce these drifter trajectories by resolving the mesoscale variability in this region. By successfully simulating the 2010 drifter trajectories, we applied the "tuned" model parameters to conduct the data assimilation experiment for the 2009 experiments and then used the model-predicted field to track reversely the body and debris to the time of the LKP. This approach worked well for this search based on the comparison between the model-predicted and the reported location of AF447 on the seafloor during the fourth search.

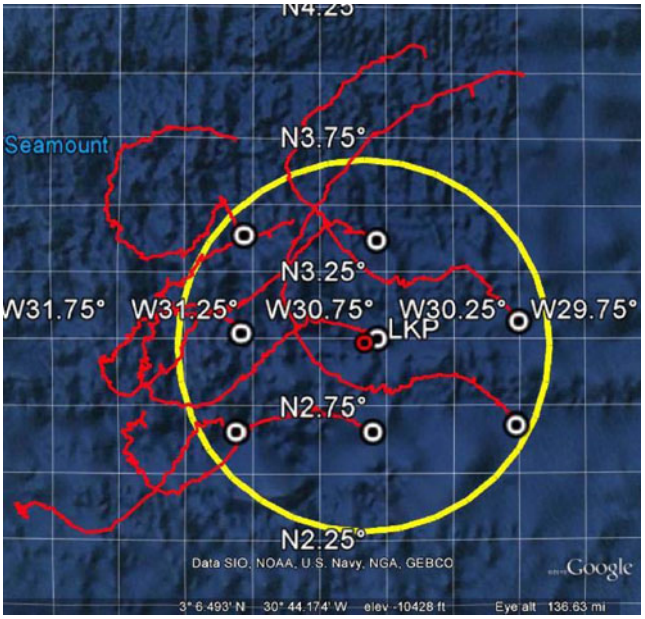

Fig. 5 Locations of the 2010 BEA surface drifter deployments (*white circles/black cores*), the airplane last known position (*LKP*, a *red circle with a black core*), a circle with a 40-nm radius drawn around the LKP (*yellow*), and the GPS drifter tracks (*red*) from June 3 to 10, 2010

3 The model validation results

3.1 The 2010 drifter trajectories

The model was capable of reproducing the eight observed drifter and model-predicted trajectories for the period from June 3 to 27, 2010 (Fig. 6). The 2010 drifter tracks were complex and the FVCOM model reproduced the observed tracks quite well in general on timescales of <10 days. After 14 days, an accumulating error in the comparison of observed and model positions was observed, but not for all drifters.

Drifter A was deployed southeast of the LKP of AF447, and both the drifter and model showed an elongated clockwise eddy about 100×200 km. The observed/predicted comparison was good and the error was about 22 km after 12 days. *Drifter B* was deployed about 36 km south of the LKP and showed the poorest comparison with the model. The error was about 150 km after 24 days. *Drifter C* was deployed about 62 km southwest of the LKP and the model track compared well (see the small loop), but the speed was slower. Note that the model C track was similar to the model B track, indicating the large variability in the ocean here on short spatial scales. The total error was about 50 km after 24 days. *Drifter D* was deployed 50 km west of the LKP and the comparison was good for 7 days, and then the error accumulated. The error was about 10 km after 8 days. *Drifter E* was deployed 72 km northwest of the LKP and the comparison was very good for about 12 days. The error was about 10 km after 12 days. *Drifter F* was deployed

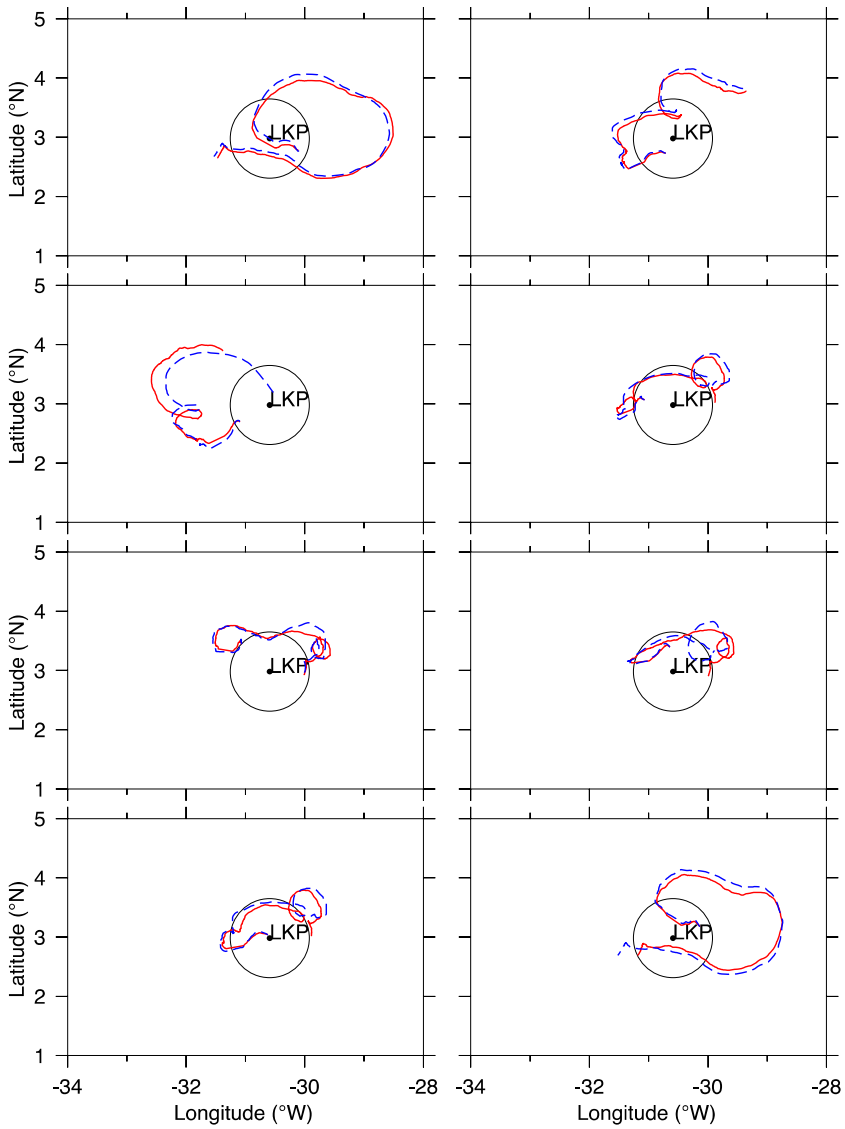

Fig. 6 Comparison of observed (*red*) and model-simulated (*blue dashed*) drifter trajectories from June 3 to 27, 2010

44 km north of the LKP and the track was similar to drifter E. The error was about 10 km after 12 days. *Drifter G* was deployed at the LKP and the model reproduced this observed track quite well over 18 days. The error was about 10 km after 18 days. *Drifter H* was deployed 64 km east of the LKP and the model comparison was good for 17 days. The error was about 15 km after 14 days.

We initially found a lack of sufficient spatial resolution in the observed data, and the success in reproducing the observed flow field depended on the correlation scale selected in the data assimilation. Each current vector derived from drifters was like an adaptive sampling along a drifter trajectory. It was easy to reproduce a trajectory, but difficult to separate all drifters in the region when the currents were dominated by the mesoscale variability. When the correlation scale is larger than 50 km, the model can only capture the observed trajectories of drifters A, C, and H, but not others. By reducing the correlation scale gradually, we found that the best solution is found at a correlation scale of ~50 km. This suggests that the correlation scale of 1° used in previous experiments for the modeling experiments used to guide the third search was too large to resolve the mesoscale variability. This was probably a reason why all models in the phase 3 search predicted a possible location of AF447 northwest of the LKP and led to the failure to locate AF447 on the seafloor.

3.2 The 2009 simulations

Applying a correlation scale of 50 km into the data assimilation method, we constructed the June 2009 flow field by assimilating all drifter data at the surface and drogued at a depth of 15 m as well as the fishermen drifters (with unknown drogue depths) into the model. An assumption was made that all these drifters were in the mixed layer. We have collected all available temperature and salinity profiles in

2009 and assimilated them into the model. In May and June 2009, there were many profiles available in that region. The thickness of the surface mixed layer varied with latitude, in the range of 30–60 m (Fig. 7). In the area close to LKP, the temperature profiles recorded by ARGO drifters showed that the surface mixed layer in that area was about ~40 m. We have added the Price–Weller–Pinkle mixed layer model into FVCOM and used it to determine the mixed layer depth. This depth was used to determine how deep the SST assimilation should go in the vertical.

With success in reproducing the mixed layer depth, the model, in general, was robust to capture the observed trajectories of most drifters and floats. Comparisons were made for all ARGO, AOML, and fishermen drifters under the three types of wind conditions (Figs. 8, 9, and 10). The error increased with time. After June 10, the model even failed to reproduce the trajectories of some AOML floats. This suggests that the reverse debris tracking was more reliably accurate in the early June, so that we should not consider the debris found after June 10, 2009, in the reverse tracking. Based on this result, we only considered the debris and bodies found on June 6–8, 2009, in our Lagrangian tracking experiments used to determine the possible location of AF447.

4 Reverse debris tracking results

The experiments were made with Blend, WRF, and ECMWF wind forcing conditions. The reverse tracking was carried out in the model-predicted flow field for bodies found on June 6–7, 2009, and debris found on June 5–7, 2009. Four cases were considered for each type of wind condition: (a) no wind drag, (b) 1 % wind drag, (c) 2 % wind drag, and (d) 3 % wind drag. The flow field used for body and debris tracking was the assimilate field with and without the inclusion of the current–wave interaction.

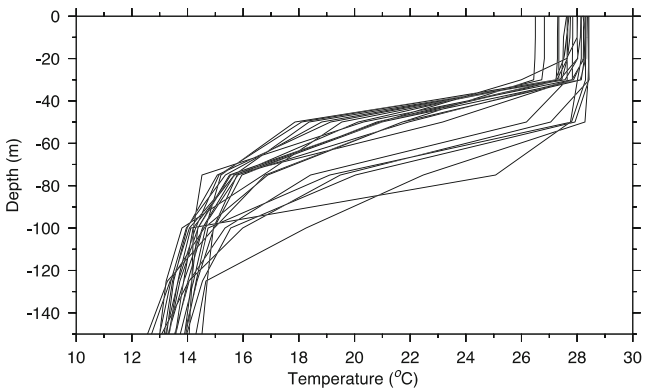

Fig. 7 Vertical profiles of water temperature in the region between (32° W, 2° N) and (28° W, 6° N) in May–June 2009

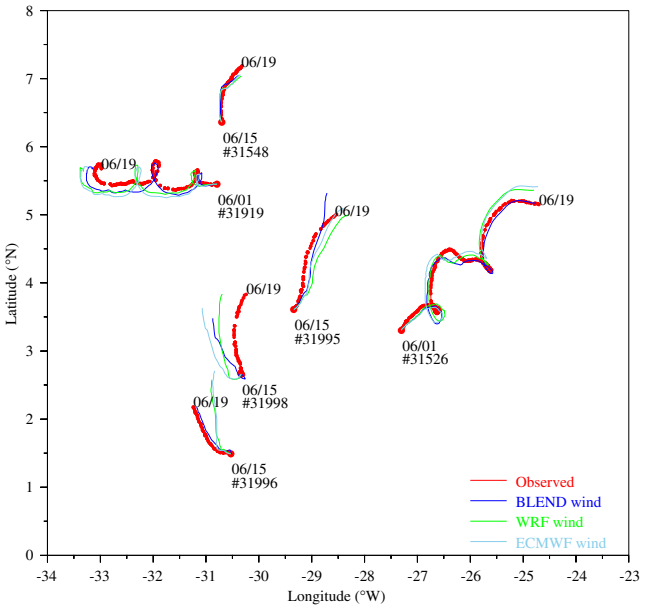

Fig. 8 Comparison of the model-predicted and the observed trajectories of AOML drifters in June 2009 for the cases with the BLEND, ECMWF, and WRF wind forcing conditions. *Number symbol* represents the drifter name. The locations of #31995, #31548, and #31919 were shifted to make the picture viewable

Figure 11 shows that the backtracked locations of bodies are significantly different for the BLEND, WRF, and ECMWF wind forcing. In spite of this, all the wind cases show common features in general. For the case with 0 % wind drag, all three cases suggested that bodies were

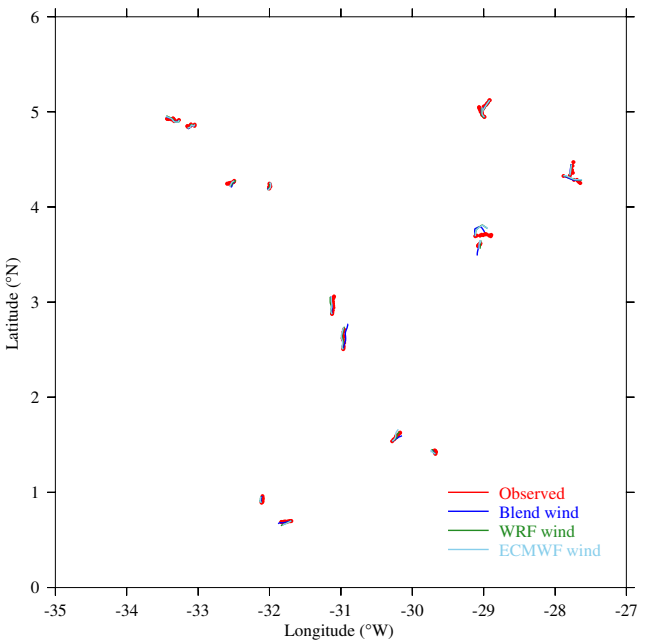

Fig. 9 Comparison of the model-predicted and the observed trajectories of Argo drifters in June 2009 for the cases with the BLEND, ECMWF, and WRF wind forcing conditions. *Red color*, observed Argo drifter trajectories

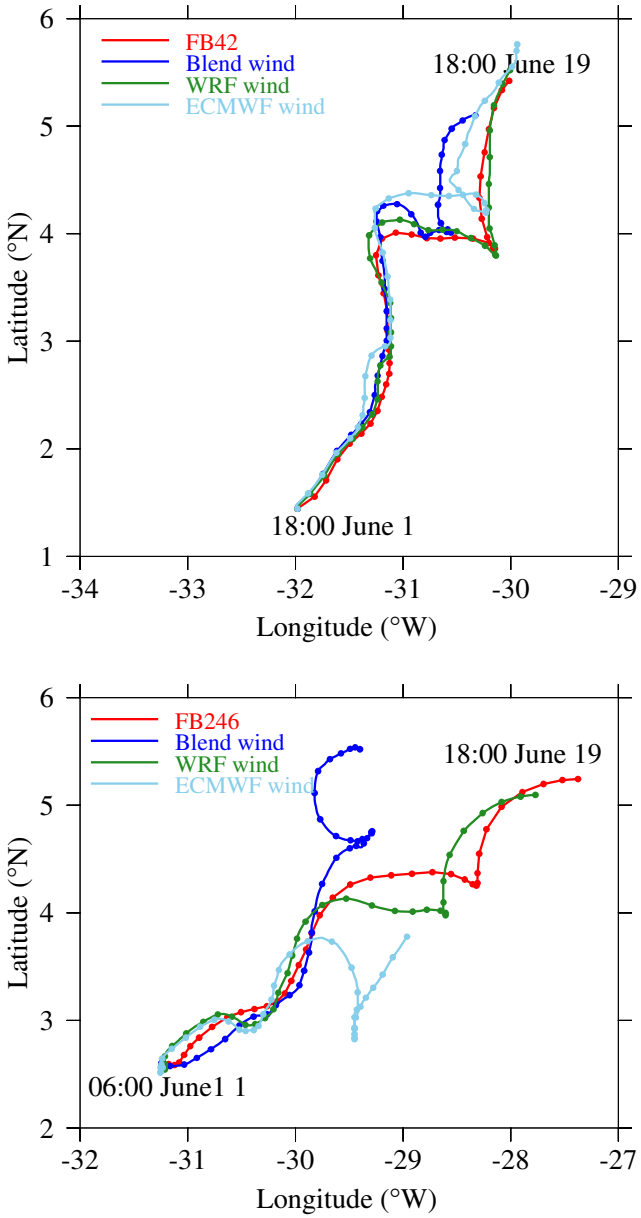

Fig. 10 Comparison of the model-predicted and the observed trajectories of BF42 and BF246 drifters in June 2009 for the cases with the BLEND, ECMWF, and WRF wind forcing conditions. *Red color*, observed BF42 drifter trajectory

originally from the northeast region with respect to LKP. In such a complex flow field, the wind drag tended to push the location southward. Because the model-predicted current field significantly differed around the ITCZ for the three types of wind forcing, the backtracked locations of bodies for these three wind cases diverged, particularly for the cases with the addition of a wind drag. It is hard to conclude which wind forcing condition was better since there were not any observed data to validate these wind fields. Instead, our experiments in the range of wind drag forcing suggested that the plane should not be located in the northwest and southwest regions far away from the LKP; also, a 3 % wind drag was too large since the model-predicted backtracked locations of bodies were outside of a 40-nm radius from the LKP.

We also tracked debris in the flow fields for the cases with BLEND, WRF, and ECMWF wind forcing. For the same wind forcing condition, the debris did not show the same backtracked locations as the bodies, even though they were in general in the same area. Differences of the backtracked locations of bodies and debris were within ~10–17 km for the BLEND wind forcing condition, ~7 km for the WRF wind forcing condition, and up to ~100 km for the ECMWF wind forcing condition. It is clear that there should be different wind drag values for bodies and debris depending on how much each object was submerged, i.e., the ratio of each object's surface area above and below the water surface. For this reason, we believed that the area predicted by body tracking was more reliable than the area predicted by debris tracking.

We have combined the backtracked locations of bodies for four direct wind drags (0, 1, 2, and 3 % wind speed) under three different types of the wind forcing to create a possibility map, with the density of estimates within 8×8-km boxes being contoured with color on a base map showing 20- and 40-nm range rings from the LKP (Fig. 12). In Fig. 12, four high-density areas were predicted by this ensemble estimate: (1) likely in the NE quadrant of the 40-nm circle centered on the LKP; (2) in a region 20–28 nm northeastward of the LKP; (3) in an area 20 nm southward of the LKP; and (4) a southeastern area outside of the 40-nm circle. Curiously increased wind drag shifted the estimated locations to the south where we see the third and fourth highest location densities. Modeling continuous wind drags instead of discrete wind drags would probably result in a ridge of hot spots extending northeastward and southeastward from the LKP instead of the island hot spots. According to the weather conditions at the time of the crash, it was unlikely for a plane to make a sharp U-turn to fly back to the third and fourth high-density areas. For this reason, the model suggested that the plane was highly likely in either near the LKP or the northeast area about 20–28 nm from the LKP.

5 Discussions

The model suggested two areas where AF447 was highly likely located. This helped the WHOI REMUS AUV Operations Group to narrow their search areas during the fourth search. The AF447 was located by the WHOI AUV Operations Group on the seafloor at approximately 3°3′ N, 30° 33′ W. This location was in the area predicted by the FVCOM estimate of the trackbacked locations of the bodies

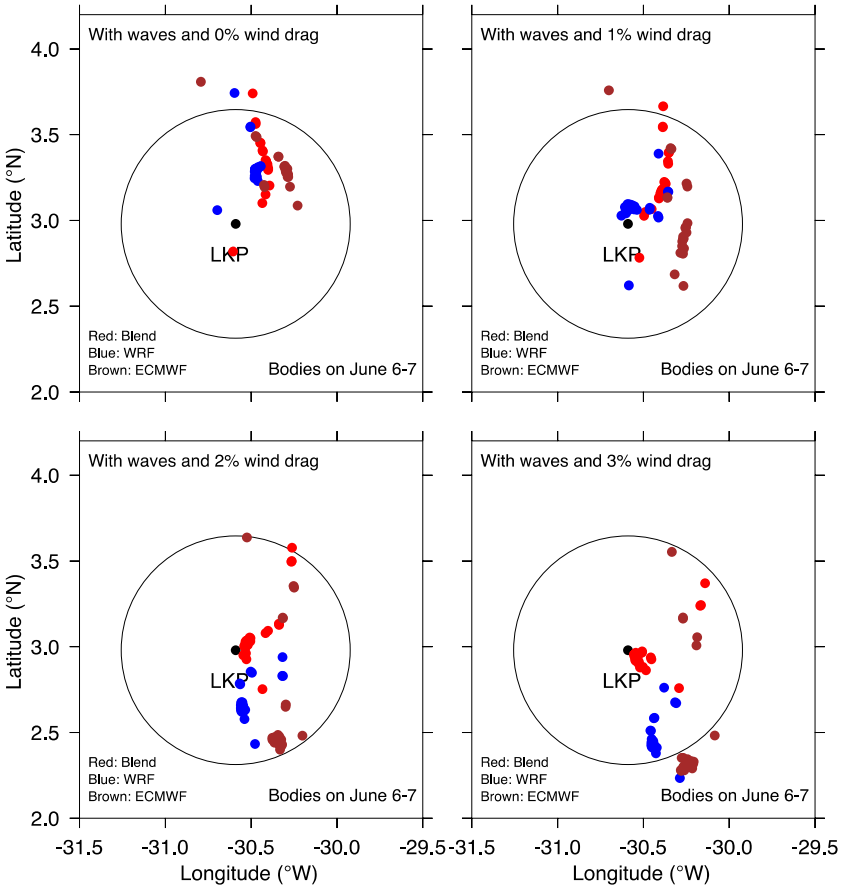

Fig. 11 Backtracked locations of bodies (found on June 6–7, 2009) at 02:00 AM on June 1, 2009, for the cases with 0, 1, 2, and 3 % wind drags. *Colors* represent the cases with the BLEND (*red*), WRF (*blue*), and ECMWF (*brown*) wind forcings

using WRF winds with a 1 % of the wind speed direct drag on the floating bodies (Fig. 13). Since the flow field significantly differed under the BLEND, WRF, and ECMWF wind conditions, this suggests that the high-resolution

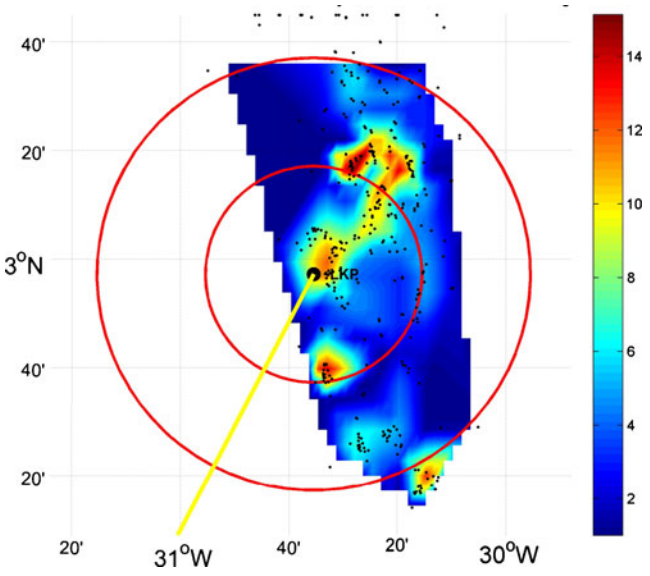

Fig. 12 Backtracked June 1 location density/8 km^2 from the combined three wind data sets and four direct wind drags on the debris and bodies with surface wave forcing included in FVCOM. The last known position (*LKP*) is in the center of 20- and 40-nm range rings

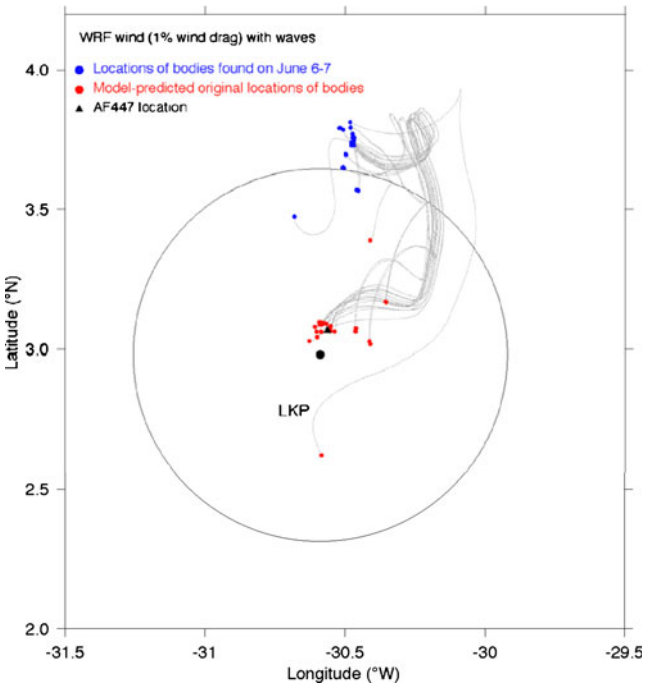

Fig. 13 Backtracked June 1 locations from the WRF wind data including surface waves and 1 % direct wind drags on the bodies with surface wave forcing included in FVCOM. The last known position (*LKP*) is in the center of the 40-nm range ring; the final location of AF447 is shown

WRF model seems to provide the more accurate surface wind forcing for this exercise. For the case with the data assimilation of all drifter and float-derived currents into the model, the wind drag was partially taken into account through the data assimilation so that 1 % of the wind drag worked well for this case. In addition to helping locate the possible location of AF447 on the seafloor, our modeling efforts provided several key findings that might be useful for a future search in that area. In the 2010 experiment, we found that without data assimilation, the model would not be able to reproduce the trajectories of drifters. The trajectories can be simulated when assimilation is used. To capture all drifter trajectories in such a small region, a correlation scale of 50 km or less was required in the assimilation. In the 2009 experiments, we have run the model under different wind (BLEND, WRF, and ECMWF) conditions for the cases with and without inclusion of the current–wave interaction. We found that by refining the model grid to ~7–10 km, the model shows a complex mesoscale flow field that varied significantly under different wind conditions. By using a correlation scale of 50 km, we were able to include all observed drifter data in the assimilation. The possible location of the plane was mostly likely in the northeast quadrant of the 40-nm circle centered on the LKP, but the possible locations shifted southward as the wind drag forcing was increased. The impact of the current–wave interaction was small in the BLEND and WRF wind cases, but large in the ECMWF wind case. The maximum difference between the wind cases with and without inclusion of the current–wave interaction was ~10–17 km in the BLEND wind case, ~7 km in the WRF wind case, but could be ~100 km in the ECMWF wind case.

6 Conclusions

The global–local nested FVCOM system, equipped with the data assimilation of SST, SSH, and drifter/float-derived currents, was capable of predicting the possible location of AF447 in the western equatorial region of the North Atlantic Ocean. With a success in reproducing the observed tracks of drifters deployed in June 2010, the model suggested that the optimal interpolation data assimilation approach with a correlation scale of 50 km was able to resolve the mesoscale variability of surface currents in the accident area. Applying this correlation scale to assimilate the drifter- and float-derived currents into the model with the assimilated surface mixed layer, the model helped narrow the search area into two possible locations. The best results were obtained by using the WRF winds and a direct wind drag of 1 % on the floating bodies. Lack of detailed knowledge of the submergence of the various general floating debris gave large errors due to the unknown direct wind drag.

References

Burchard H (2002) Applied turbulence modeling in marine waters. Springer, Berlin, 215 pp

Chen C, Liu H, Beardsley R (2003) An unstructured grid, finite-volume, three-dimensional, primitive equations ocean model: application to coastal ocean and estuaries. J Atmos Ocean Technol 20(1):159–186

Chen C, Wu Z, Beardsley RC, Shu S, Xu C (2005) Using MM5 to hindcast the ocean surface forcing fields over the Gulf of Maine and Georges Bank region. J Atmos Ocean Technol 22(2):131–145

Chen C, Beardsley RC, Cowles G (2006a) An unstructured grid, finite-volume coastal ocean model (FVCOM) system. Special Issue entitled "Advance in Computational Oceanography". Oceanography 19(1):78–89

Chen C, Beardsley RC, Cowles G (2006b) An unstructured grid, finite-volume coastal ocean model-FVCOM user manual, 2nd edn. School for Marine Science and Technology, University of Massachusetts Dartmouth, New Bedford. Technical report SMAST/UMASSD-06-0602, 318 pp

Pietrzak JJ, Jakobson B, Burchard H, Vested HJ, Petersen O (2002) A three-dimensional hydrostatic model for coastal and ocean modeling using a generalized topography following co-ordinate system. Ocean Model 4:173–205

Smagorinsky J (1963) General circulation experiments with the primitive equations. I. The basic experiment. Mon Weather Rev 91:99–164